Published in "Physical Review B: Condensed Matter and Materials Physics
76 (11): 115118, 2007" which should be cited to refer to this work.

Phases and phase transitions in the half-filled t-t' Hubbard chain

G. I. Japaridze,[1] R. M. Noack,[2] D. Baeriswyl,[3] and L. Tincani[2]
[1]*Andronikashvili Institute of Physics, Tamarashvili 6, 0177 Tbilisi, Georgia*
[2]*Fachbereich Physik, Philipps-Universität Marburg, D-35032 Marburg, Germany*
[3]*Département de Physique, Université de Fribourg, CH-1700 Fribourg, Switzerland*

We study the quantum phase transition from an insulator to a metal realized at $t'=t'_c>0.5t$ in the ground state of the half-filled Hubbard chain with both nearest-neighbor (t) and next-nearest-neighbor (t') hopping. The study is carried out using the bosonization approach and density-matrix renormalization-group calculations. An effective low-energy Hamiltonian that describes the insulator-metal transition is derived. We find that the gross features of the phase diagram are well described by the standard theory of commensurate-incommensurate transitions in a wide range of parameters. We also obtain an analytical expression for the insulator-metal transition line $t'_c(U,t)$. We present results of density-matrix-renormalization-group calculations of spin and charge distribution in various sectors of the phase diagram. The numerical results support the picture derived from the effective theory and give evidence for the complete separation of the transitions involving spin and charge degrees of freedom.

I. INTRODUCTION

During the past decades, the Mott metal-insulator transition has been the subject of great interest.[1–3] In the canonical model for this transition—the single-band Hubbard model—the origin of the insulating behavior is the on-site Coulomb repulsion between electrons. For an average density of one electron per site, the transition from the metallic to the insulating phase is expected to occur when the electron-electron interaction strength U is of the order of the delocalization energy (which is a few times the hopping amplitude t). The critical value $(U/t)_c$ turns out to be quite independent of the specific band structure.[4] It is important to recall that the Mott transition is often preceded by antiferromagnetic ordering, which usually leads to insulating behavior and thus masks the Mott phenomenon.

While the underlying mechanism driving the Mott transition is by now well understood, many questions remain open, especially about the region close to the transition point where perturbative approaches fail to provide reliable answers. The situation is more fortunate in one dimension, where nonperturbative analytical methods together with well-controlled numerical approaches allow us in many cases to determine both the ground state and the low-lying excited states.[5–7] However, even in one dimension, apart from the exactly solvable cases, a full treatment of the fundamental issues related to the Mott transition still constitutes a hard and long-standing problem.

In this paper, we study the t-t' Hubbard chain which includes both nearest, t, and next-nearest-neighbor, t', hopping terms. We limit ourselves to an average density of one electron per site (the half-filled band case). Depending on the ratio between t' and t, the system has two or four Fermi points. Correspondingly, it shows one- or two-band behavior and has a rich phase diagram. Therefore, it is not surprising that the model has been the subject of intensive analytical and numerical studies, including a weak-coupling renormalization group analysis,[8] density-matrix-renormalization-group (DMRG) calculations for charge and spin gaps,[9–13] the electric susceptibility,[14] the momentum distribution function,[15–17] and the conductivity[13] as well as, very recently, a variational technique.[18]

Unfortunately, conflicting results have been reported for the transition region, in particular, regarding the character of the transition, the number of different phases, and the number of gapless modes. In this paper, we hope to settle some of the unresolved issues using a combined analytical and numerical analysis. We focus our attention on the insulator-metal transition as a function of t' for a fixed on-site repulsion U. An effective continuum theory allows us to show that in the parameter range $0.5t<t'<t'_c$ the system exhibits the characteristic behavior of a commensurate-incommensurate transition.[19] Close to the transition point, additional scattering processes characteristic of two-band behavior[8] set in. We argue that these processes induce a crossover to Kosterlitz-Thouless-type critical behavior, as found in Ref. 14. The numerical analysis also allows us to study the gaps in the excitation spectrum as well as the charge and spin-density distributions.

The paper is organized as follows. In Sec. II, general properties of the model including the strong-coupling limit and the structure of the phase diagram are briefly reviewed. Section III discusses the metal-insulator transition from the point of view of a weak-coupling bosonization approach, which leads to the quantum sine-Gordon field theory, the standard model for commensurate-incommensurate transitions. The critical line obtained is then compared with that obtained from numerical calculations. The behavior of the numerically obtained spin and charge gaps is presented and discussed in terms of the bosonization picture. In Sec. IV, spin-charge separation in various phases is explored via numerical results for the Fourier transform of the local charge density in the ground state and the local spin density in the excited spin triplet state. Special attention is given to the regime of large t' where the model represents a system of two coupled chains. Section V summarizes and concludes.

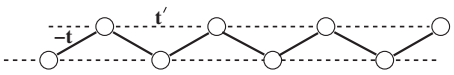

FIG. 1. The t-t' Hubbard chain.

II. t-t' HUBBARD CHAIN

The one-dimensional t-t' Hubbard model is defined by the Hamiltonian

$$\mathcal{H} = -t\sum_{j,\sigma}(c^{\dagger}_{j,\sigma}c_{j+1,\sigma} + c^{\dagger}_{j+1,\sigma}c_{j,\sigma}) + t'\sum_{j,\sigma}(c^{\dagger}_{j,\sigma}c_{j+2,\sigma} + c^{\dagger}_{j+2,\sigma}c_{j,\sigma}) + U\sum_{j,\sigma}(n_{j,\uparrow}-1/2)(n_{j,\downarrow}-1/2), \quad (1)$$

where $c^{\dagger}_{j,\sigma}(c_{j,\sigma})$ are electron creation (annihilation) operators on site j with spin projection $\sigma=\uparrow,\downarrow$, $n_{j,\sigma}=c^{\dagger}_{j,\sigma}c_{j,\sigma}$, and U is the on-site Coulomb repulsion.

The model can be viewed either as a single chain with both nearest- and next-nearest-neighbor hoppings or, as illustrated in Fig. 1, as a system of two coupled chains. The former view is appropriate for $t \gg t'$, the latter for $t' \gg t$.

For $t'=0$, we recover the ordinary Hubbard model which is exactly (Bethe ansatz) solvable.[5] In the case of a half-filled band, the ground state is insulating for arbitrary positive values of U; the charge excitation spectrum is gapped while the spin excitation spectrum is gapless.[5,6] For $U \ll t$ the charge gap Δ_c is exponentially small, $\Delta_c \approx \sqrt{Ut}e^{-2\pi t/U}$, while $\Delta_c \approx U$ for $U \gg t$.[6]

For $t' \neq 0$ the model is no longer integrable except in the noninteracting limit, $U=0$, where H is diagonalized by Fourier transformation and has a single-electron spectrum

$$\varepsilon(k) = -2t\cos k + 2t'\cos 2k. \quad (2)$$

For $t' < 0.5t$, the electron band has two Fermi points at $k_F = \pm\pi/2$, separated from each other by the umklapp vector $q=\pi$ (see Fig. 2). In this case, a weak-coupling renormalization group analysis[8] predicts the same behavior as for $t'=0$ because the umklapp term of order U is not modified; it again leads to the dynamical generation of a charge gap for $U>0$, while the magnetic excitation spectrum remains gapless. Note that the stability of the Mott insulating phase with respect to the weak perturbation caused by the next-nearest-neighbor hopping is an intrinsic feature of the one-dimensional system, where the topology of the Fermi surface remains unchanged for $t' < 0.5t$. For instance, for the two-dimensional half-filled t-t' Hubbard model, the ideal nesting of the square Fermi surface at $t'=0$ is broken by an arbitrarily small $t' \neq 0$, thereby destroying the insulating behavior for $U \to 0$.[20]

In the strong-coupling limit, $U \gg t, t'$, the charge sector is gapped, while the spin sector can be mapped onto a frustrated Heisenberg chain

$$H = \sum_j (J\mathbf{S}_j \cdot \mathbf{S}_{j+1} + J'\mathbf{S}_j \cdot \mathbf{S}_{j+2}), \quad (3)$$

with $J=4t^2/U$ and $J'=4t'^2/U$. This model has been extensively studied using a number of different analytical methods[21–23] and has been found to develop a spin gap for $J'/J \sim (t'/t)^2 > 0.2412$,[21,22] and incommensurate antiferromagnetic order for $J'/J > 0.5$.[23] This picture has been confirmed numerically.[11,12]

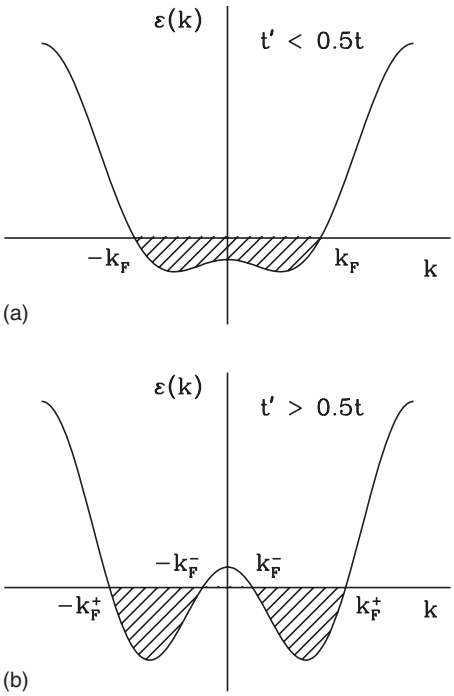

FIG. 2. Single-particle dispersion relation of the t-t' chain for (a) $t'=0.4t$ and (b) $t'=t$.

For $t' > 0.5t$, the Fermi level intersects the one-electron band at four points $(\pm k_F^{\pm})$. This is the origin of more complex behavior for weak and intermediate values of U. For weak coupling $(U \ll t)$, the ground-state phase diagram is well understood in the two-chain limit $(t' \gg t)$.[8] In this case, the Fermi vectors $k_F^{\pm}$ are sufficiently far from $\pi/2$ to suppress first-order umklapp processes. Therefore, the system is metallic. The infrared behavior is governed by the low-energy excitations in the vicinity of the four Fermi points, in full analogy with the two-leg Hubbard model.[24] Thus, while the charge excitations are gapless, the spin degrees of freedom are gapped.[8,12,13,15,24] Higher-order umklapp processes become relevant for intermediate values of U because the Fermi momenta fulfill the condition $4(k_F^+ - k_F^-) = 2\pi$ (at half-filling). Therefore, starting from a metallic region for small U at a given value of t' $(t' > 0.5t)$, one reaches a transition line $U=U_c(t')$, above which the system is insulating with both charge and spin gaps.[8] The gross features of the phase diagram are depicted in Fig. 3.

III. METAL-INSULATOR TRANSITION

A. Bosonization

We first consider the regime $U, t' \ll t$ where bosonization is applicable. We linearize the spectrum in the vicinity of the two Fermi points $k_F = \pm\pi/2$ and go to the continuum limit by substituting

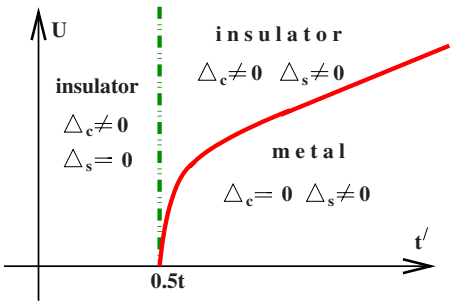

FIG. 3. (Color online) Qualitative sketch of the ground-state phase diagram of the half-filled t-t' model. The solid line marks the metal-insulator transition. The dashed line indicates the transition from a gapless spin excitation spectrum at $t' \leqslant 0.5t$ to the spin-gapped phase.

$$c_{n\sigma} \to i^n \psi_{R\sigma}(x) + (-i)^n \psi_{L\sigma}(x), \tag{4}$$

where the operators $\psi_{R\sigma}(x)$ and $\psi_{L\sigma}(x)$ are the right and left components of the Fermi field, respectively. These fields can be bosonized in a standard way,[25]

$$\psi_{R\sigma} \to \frac{1}{\sqrt{2\pi\alpha}} e^{i\sqrt{4\pi}\phi_{R\sigma}},$$

$$\psi_{L\sigma} \to \frac{1}{\sqrt{2\pi\alpha}} e^{-i\sqrt{4\pi}\phi_{L\sigma}}, \tag{5}$$

where $\phi_{R\sigma}$ ($\phi_{R\sigma}$) are the right(left)-moving Bose fields and α is the infrared cutoff. We define $\phi_\sigma = \phi_{R\sigma} + \phi_{L\sigma}$ and introduce linear combinations, $\varphi_c = (\phi_\uparrow + \phi_\downarrow)\sqrt{2}$ and $\varphi_s = (\phi_\uparrow - \phi_\downarrow)\sqrt{2}$, to describe the charge and spin degrees of freedom, respectively. Correspondingly, we introduce the conjugate fields $\theta_\sigma = \phi_{L\sigma} - \phi_{R\sigma}$ and $\vartheta_c = (\theta_\uparrow + \theta_\downarrow)\sqrt{2}$ and $\vartheta_s = (\theta_\uparrow - \theta_\downarrow)\sqrt{2}$. After some standard algebra, we arrive at the bosonized version of the Hamiltonian (1) as follows:

$$\mathcal{H} = \mathcal{H}_s + \mathcal{H}_c,$$

where both the spin part

$$\mathcal{H}_s = v_s \int dx \left[\frac{1}{2}(\partial_x \varphi_s)^2 + \frac{1}{2}(\partial_x \vartheta_s)^2 + \frac{m_s^0}{2\pi\alpha^2} \cos(\sqrt{8\pi}\varphi_s) \right], \tag{6}$$

and the charge part,

$$\mathcal{H}_c = v_c \int dx \left[\frac{1}{2K_c}(\partial_x \varphi_c)^2 + \frac{K_c}{2}(\partial_x \vartheta_c)^2 + \frac{m_c^0}{2\pi\alpha^2} \cos(\sqrt{8\pi}\varphi_c) \right], \tag{7}$$

are described by the massive sine-Gordon model, with parameters

$$v_s \approx v_c \approx v_F,$$

$$(K_c - 1) = -2m_s^0 = 2m_c^0 \approx -U/\pi t. \tag{8}$$

There is an important difference between H_s and H_c due to the different stiffness constants. In the spin sector with $K_s = 1$, the system is in the weak-coupling limit and scales to a Gaussian model with gapless spin excitations. In the charge sector with $K_c < 1$, the system is in the strong-coupling regime and the low-energy behavior is dominated by the cosine term. In the ground state, the field φ_c is pinned at one of the minima of the cosine term and, correspondingly, there is a finite energy gap for charge excitations.

Let us now discuss what happens when t' increases and reaches values of the order of $t/2$, where two additional Fermi points appear in the band structure. For spin degrees of freedom, new scattering channels appear at $t' = t/2$, and the system scales to strong coupling. Therefore, a spin gap is expected to open for $t' > t/2$, very much like in the case of two coupled Hubbard chains.[24]

For the charge degrees of freedom, the situation is more complicated (and more interesting) because the charge gap blocks new scattering channels until t' is made sufficiently large so that additional states emerge beyond the gapped region. Thus, for t' slightly above $t/2$, the (bare) Fermi momentum changes without affecting the umklapp processes. To discuss this phenomenon, it is useful to measure the single-particle energies with respect to the Fermi energy

$$\varepsilon_F = \begin{cases} -2t', & t' < 0.5t \\ \dfrac{-t^2}{2t'}, & t' > 0.5t. \end{cases} \tag{9}$$

In addition, the bosonized version of the single-particle part of the Hamiltonian introduces a chemical potential term $-2t'\sqrt{2/\pi}\int dx \partial_x \varphi_c$. In order to allow for a change of the particle number around the Fermi points $\pm\pi/2$, we therefore have to add a topological term

$$\delta H_c = -\mu_{\text{eff}} \sqrt{\frac{2}{\pi}} \int dx \partial_x \varphi_c, \tag{10}$$

where

$$\mu_{\text{eff}} = \begin{cases} 0 & \text{for } t' < 0.5t \\ \dfrac{t^2}{2t'} - 2t' \neq 0 & \text{for } t' > 0.5t. \end{cases} \tag{11}$$

The Hamiltonian $H_c + \delta H_c$ is the standard one for the commensurate-incommensurate transition,[25,26] and has been intensively studied in the past using bosonization[19] and the Bethe ansatz.[27]

We now apply the theory of commensurate-incommensurate transitions to the insulator-metal transition as a function of t'. At $\mu_{\text{eff}} = 0$ and $K_c < 1$, the ground state of the field φ_c is pinned at

$$\langle 0 | \sqrt{8\pi}\varphi_c | 0 \rangle_0 = 2\pi n. \tag{12}$$

The presence of the effective chemical potential makes it necessary to consider the ground state of the sine-Gordon model in sectors with nonzero topological charge. Using the

standard expression for the charge density in the case of two Fermi points,[25]

$$\rho_c(x) \simeq \frac{1}{\sqrt{2\pi}}\partial_x\varphi_c + A_{2k_F}\cos(2k_F x)\sin(\sqrt{2\pi}\varphi_c)\cos(\sqrt{2\pi}\varphi_s) + A_{4k_F}\cos(4k_F x)\cos(\sqrt{8\pi}\varphi_c), \quad (13)$$

we observe that the pinning of the field φ_c in one of the minima (12) suppresses the $2k_F$ charge fluctuations and stabilizes the $4k_F$ component. Any distortion of the $4k_F$ charge distribution would require an energy greater than the charge gap. This competition between the chemical potential term and commensurability drives a continuous phase transition from a gapped (insulating) phase at $\mu_{\rm eff} < \mu^c_{\rm eff}$ to a gapless (metallic) phase at

$$\mu_{\rm eff} > \mu^c_{\rm eff} = \Delta_c, \quad (14)$$

where Δ_c is the charge gap at $\mu_{\rm eff}=0$.

We now separately consider the qualitative behavior of the system in the following three parameter regimes: (i) $t' < 0.5t$, (ii) $0.5t < t' < t'_c$, and (iii) $t' > t'_c$. In regime (i), $t' < 0.5t$, we expect a charge gap $\Delta_c(U,t') \approx \Delta_c(U,t'=0)$ and no spin gap, as in the simple Hubbard model ($t'=0$). In regime (ii), $0.5t < t' < t'_c$, the spin gap opens while the charge gap is reduced as[28]

$$\Delta_c(U,t') = \Delta_c(U,0.5t) - \mu_{\rm eff}, \quad (15)$$

where $\mu_{\rm eff}$ is given by Eq. (11). Therefore, the charge gap decreases with increasing t' and tends to zero at a t'_c qualitatively given by

$$\Delta_c(U,0) - 2t'_c + t^2/2t'_c = 0. \quad (16)$$

In regime (iii), $t' > t'_c$, the behavior of the system is characterized by four Fermi points, $\pm k^{\pm}_F$. The charge excitations are gapless, while the spin excitations are, generically, gapped.[8,24] Charge fluctuations will be characterized by two dominant periodic modulations with wave vectors $2k^-_F$ and $2k^+_F$. For t' slightly larger than t'_c, the usual charge-density wave ($2k^+_F \approx \pi$) is accompanied by a long-wavelength modulation at $2k^-_F$.

Note that the closing of the charge gap is directly connected with the appearance of a "hole bag" at small momenta $|k| < k^-_F$, which is compensated (at half-filling) by the creation of occupied states at $\pi/2 < |k| < k^+_F$. (This will be discussed in more detail in Sec. III C below.) Such a redistribution of occupied states in momentum space is generic for a transition in which the dynamically generated gap competes with some external parameter which tries to shift the system from the distribution most favored for gap formation. For example, in the case of the standard repulsive Hubbard model at half-filling, the chemical potential tries to shift the Fermi momenta of the system from the commensurate values $\pm\pi/2$, where the umklapp scattering processes responsible for the charge gap formation are relevant.[25] In the t-t' Hubbard model, the same effect takes place via an increase of the next-nearest-neighbor hopping amplitude t'. Therefore, the gross features of the metal-insulator transition in the t-t' Hubbard model are similar to those of the standard commensurate-incommensurate transition.

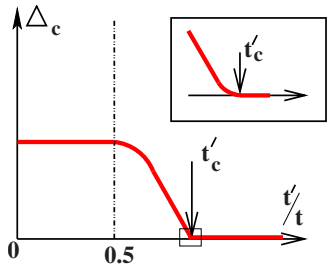

FIG. 4. (Color online) Sketch of the charge gap as a function of the parameter t'. The inset shows an enlargement of the vicinity of the transition point.

However, there is one important aspect which makes the metal-insulator transition in the t-t' Hubbard model different from the case of the standard Hubbard chain. In marked contrast to the latter case, the metal-insulator transition in the t-t' Hubbard chain is not associated with a change in the band filling. Therefore, the "effective" chemical potential is not an external parameter, but is instead determined by the hopping amplitudes t and t'. As a result, the change in the topology of the Fermi surface does not lead to complete suppression of the scattering processes responsible for the charge gap formation. Near the transition point, where the charge gap generated by the standard umklapp scattering processes vanishes, states in the vicinity of $k=0$ will start to contribute to higher-order umklapp scattering processes. These processes are responsible for the opening of a charge gap with increasing U in the two-band limit, i.e., when $t' \gg t$.[8] Therefore, a crossover to the regime of two-band behavior takes place in the parameter range where the renormalized one-band (Hubbard) gap (15) becomes exponentially small. Therefore, the linear decay of the charge gap as a function of t' crosses over to exponential behavior. The evolution of the charge gap as a function of t' is sketched in Fig. 4.

B. Transition line

In order to investigate the detailed behavior of the metal-insulator transition and to test the validity of the picture obtained from bosonization, we have carried out numerical calculations using the DMRG.[29]

We have calculated the properties of the ground-state and low-lying excited states for systems with open boundary conditions of lengths between $L=32$ and $L=128$ sites, keeping up to $m=1000$ density-matrix eigenstates. As we shall see in the following, the finite-size effects are quite large in certain parameter regimes, so that a careful finite-size scaling must be carried out.

The critical behavior of the metal-insulator transition as a function of U/t for $t' > 0.5t$ can be obtained from the behavior of the electric susceptibility, which diverges in going from an insulator to a metal.[14,30] In Fig. 5, we display the transition line in the t-t'-U model at $t=1$ obtained from the

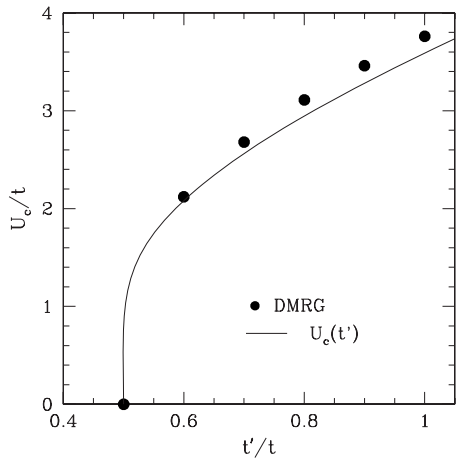

FIG. 5. The metal-insulator transition line in the t-t'-U model with $t=1$ obtained from DMRG studies (Refs. 14 and 30) (black circles) and from Eq. (16) (solid line).

DMRG[14,30] and from Eq. (16). The agreement between the DMRG results and Eq. (16) is remarkably good.

C. Momentum distribution function

In order to investigate the redistribution of occupied momentum states discussed at the end of Sec. III A, it is very instructive to examine the momentum distribution function calculated using the DMRG. The momentum distribution can be calculated by taking the Fourier transformation of the single-particle density matrix,

$$\langle n_k\rangle \equiv \frac{1}{2L}\sum_{i,\sigma}\sum_{r}\cos kr\langle c^{\dagger}_{i,\sigma}c_{i+r,\sigma}\rangle, \qquad (17)$$

with $k=\frac{2\pi}{L}n$ where $n=-L/2+1,\ldots,L/2$. Only the real part need be considered because the single-particle density matrix is even in r. In a system with periodic boundary conditions or an infinite system, the single-particle density matrix $\langle c^{\dagger}_{i,\sigma}c_{i+r,\sigma}\rangle$ would not depend on i due to translational invariance. For the open boundary conditions considered here, we carry out the average over i. While the discrete Fourier transform we use here is formally correct only for a periodic system, we find that using either an approximation to a Fourier integral or expanding in single-particle basis functions for open boundary conditions does not make a significant difference in the numerical results on the scale of the plots shown here.

In order to gauge the effect of the interactions, it is useful to compare with the momentum distribution for the noninteracting system. For $U=0$, all momentum points within the Fermi points are fully occupied, i.e., $\langle n_k\rangle=1$ only for $|k|<k_F$ for $|t'|<0.5$ and only for $k_F^-<|k|<k_F^+$ for $|t'|>0.5$, and all other k points are unoccupied, $\langle n_k\rangle=0$; see also Fig. 2.

In Fig. 6, we present the momentum distribution as a function of t' for $U=3t$. In the region $0<t'<0.6t$, $\langle n_k\rangle$ shows no qualitative differences from the $t'=0$ case. Its insulating character manifests itself as a smooth variation of $\langle n_k\rangle$ at the Fermi points $\pm\pi/2$, in contrast to the Fermi step

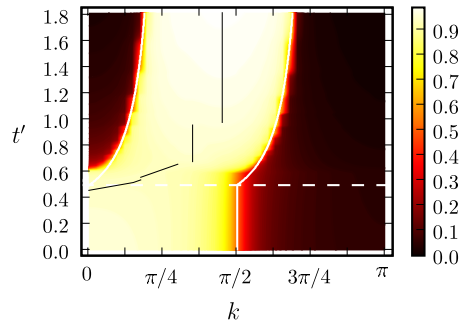

FIG. 6. (Color online) Momentum distribution $\langle n_k\rangle$ for $U/t=3$ and system size $L=80$. The white lines indicate the Fermi surface for $U=0$, and the black lines locate the maximum of $\langle n_k\rangle$.

or Luttinger liquid singularity that one would expect for a metal. States near $k=0$ begin to be removed at $t'\approx 0.6t$, significantly above the value at which the number of Fermi points changes from two to four in the noninteracting system ($t'=0.5t$). The formation of this hole pocket proceeds continuously as t' is increased further. It is accompanied by a steepening of the slope of $\langle n_k\rangle$, both near k_F^- and near k_F^+. More studies will be needed to determine the detailed behavior of the momentum distribution function close to the Fermi points in this spin-gapped two-chain regime.

We have also performed simulations at larger values of U, where the first sign of a hole pocket appears at larger values of t', following essentially the metal-insulator transition line of Fig. 5. On the insulating side of this line, $\langle n_k\rangle$ is smooth, as expected.

D. Charge and spin gaps

In order to investigate the predictions of the continuum theory, we calculate the charge gap, defined as

$$\Delta_c = \frac{1}{2}[E_0(N+2,0)+E_0(N-2,0)-2E_0(N,0)] \qquad (18)$$

and the spin gap,

$$\Delta_s = E_0(N,1)-E_0(N,0), \qquad (19)$$

where $E_0(N,S)$ is the ground-state energy for N particles and spin S on a chain of fixed length L, using the DMRG.

We will first examine the charge gap, starting with its system size dependence. In Fig. 7, we display the charge gap plotted as a function of the inverse chain length for various values of t' for $U/t=3$. As can be seen, the scaling with $1/L$ is well behaved for values of t' from 0 to 0.8. For $0\leqslant t'\leqslant 0.6t$, the scaling has a substantial positive quadratic term in $1/L$ and the gap is finite. For $t'=0.65t$ and $0.8t$, the extrapolated gap clearly vanishes and there is a negligible or negative quadratic contribution. For $t'>0.8$ (not shown), the finite-size effects become irregular due to incommensurability of the charge excitations, and finite-size extrapolation becomes difficult.

In Fig. 8, the $L=\infty$ extrapolated value of the charge gap is displayed as a function of t' for $U/t=2$ and $U/t=3$. There is

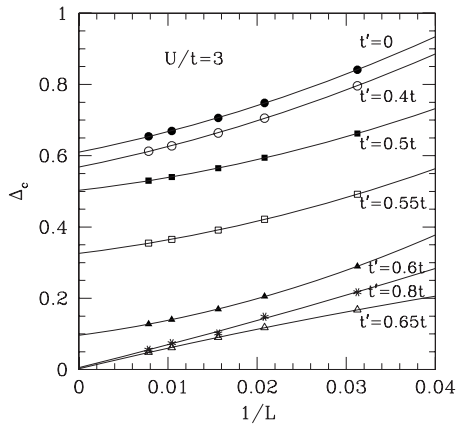

FIG. 7. Charge gap as a function of $1/L$ for $U/t=3$ and various values of t'/t.

a clearly defined insulator-metal transition at $t_c=0.55t$ at $U/t=2$ and $t_c=0.65t$ for $U/t=3$. Note that the charge gap goes smoothly to zero above $t'=0.5t$ for $U/t=3$. The inset in Fig. 8 shows the charge gap for $U/t=3$ as a function of the parameter $\mu_{\rm eff}=2t'-t^2/2t'$ for $0.5t<t'<0.85t$. As can be seen, the charge gap drops off approximately linearly with $\mu_{\rm eff}$, in agreement with Eq. (15). For $U/t=2$, there is a somewhat irregular behavior of the charge gap near the $t'=0.5t$. In particular, there is a small peak exactly at $t'=0.5$. The finite-size scaling for this point is completely regular, however, and we estimate the size of the total error, due to both the extrapolation and the DMRG accuracy, to be less than the symbol size. Therefore, in our estimation, the peak at $t'=0.5$ is a real effect. For $t'=0.55$, the value of the extrapolated charge gap is slightly below zero. This is due to errors in the finite-size extrapolation due to slightly irregular behavior with system size.

In Fig. 9, we display the spin gap as a function of t' at $U/t=2$ and $U/t=3$ for various values of the chain length L. As can be clearly seen, for $0<t'\leqslant 0.5t$ the spin excitation spectrum on finite chains does not depend on t'. For $t'\leqslant 0.5t$, the value of the spin gap is found to coincide with

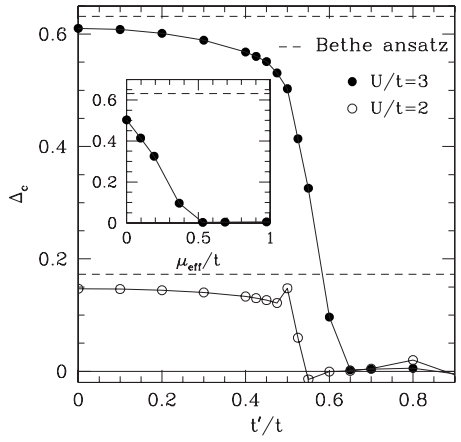

FIG. 8. Charge gap as a function of t' for $U/t=3$ (black circles) and $U/t=2$ (open circles). The inset shows the charge gap as a function of the parameter $\mu_{\rm eff}$ for $0.5<t'<0.85t$.

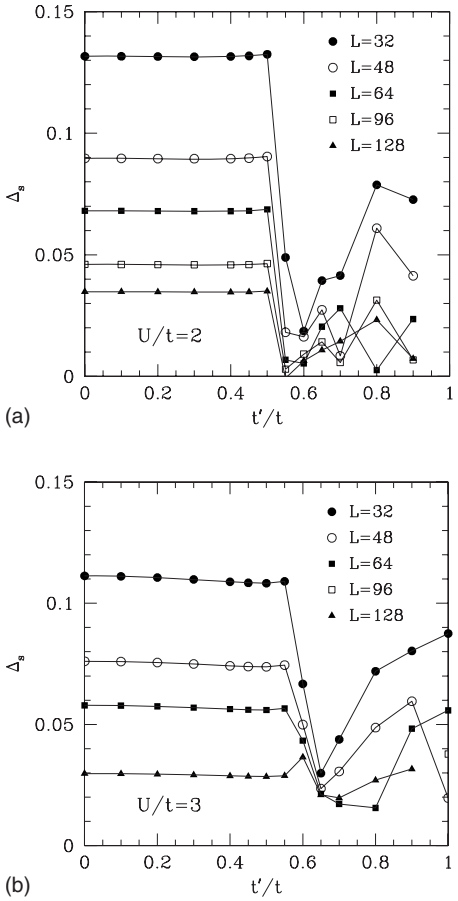

FIG. 9. Spin gap of as a function of t' for (a) $U/t=2$ and (b) $U/t=3$.

that of the half-filled Hubbard model ($t'=0$) which vanishes in the infinite-chain limit (see Fig. 10).

A clear change in the t' dependence of the spin gap at $U/t=2$ takes place at $t'=0.5t$, indicating the development of a new phase in the spin sector. It is known from other studies[8,12,13,15,24] that a spin gap opens at a critical value of t' which is approximately at or slightly above $t'=0.5t$, becoming weakly larger at intermediate U values.

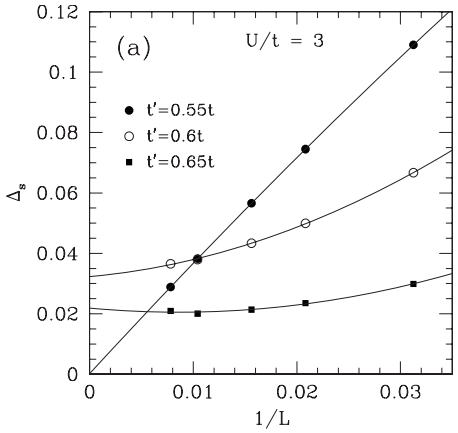

FIG. 10. Spin gap as a function of $1/L$ for $U/t=3$ and various values of t'/t.

In Fig. 10, we display the spin gap plotted as a function of the inverse chain length for three values of t' near the transition at $U/t=3$. At $t'=0.55t$, the spin gap clearly scales to zero at infinite system size, with the values at a particular system size virtually identical to the $t'=0$ case and the scaling predominantly linear in inverse system size. For $t'=0.6t$ and $t'=0.65t$, the dominant scaling term is quadratic rather than linear in $1/L$ and there is clearly scaling to a finite value of the gap. For $t'=0.65t$, the size of the extrapolated gap is smaller than for $t'=0.6t$, and there is a slight upturn in the gap at the largest system size, which, however, is not significantly larger than the estimated error of the DMRG calculation, approximately the symbol size. However, for larger values of t', the finite-size behavior becomes less regular, as can be seen in Figs. 9(a) and 9(b). This behavior is due to the appearance of an incommensurate wave vector characterizing the spin excitations that occurs when a substantial density of states at all four Fermi points develops and makes it virtually impossible to carry out a well-controlled finite-size scaling for larger values of t'.

The transition associated with the opening of the spin gap is independent of the insulator-metal transition, as can be clearly seen for $U/t=3$ (where the effect of fluctuations is reduced). As is shown in Fig. 9(b) and Fig. 10, the spin gap opens for $t'_s \geqslant 0.55t$, while the insulator-metal transition takes place at $t'_c \simeq 0.65t$ (see Fig. 8). Note that the critical value of the next-nearest-neighbor hopping amplitude, corresponding to an opening of the spin gap at $U/t=3$, $t'_s \geqslant 0.55t$, deviates from the line $t'_s \geqslant 0.5t$. Our findings agree with previous studies.[8,12,13,15,24]

E. Two-chain limit

We now discuss the limit of strong next-nearest-neighbor hopping ($t' \gg t$). For $t=0$, the system is decoupled into two half-filled Hubbard chains and, for arbitrary $U>0$, the ground state corresponds to a Mott insulator. The origin of the insulating behavior is the commensurability of umklapp scattering between the Fermi points, located at $\pm\pi/4$ and $\pm 3\pi/4$. When $t \neq 0$ this commensurability is lost. The Fermi points are shifted with respect to their values at $t=0$, and the Fermi energy (the chemical potential for $U=0$) moves away from 0 to $\varepsilon_F \approx -t^2/2t'$ (for $t \ll t'$). For large enough values of t, the system is therefore expected to be metallic.

In order to estimate the location of the Mott transition, we can use a similar argument to the one given above for $t' \approx 0.5$. As long as the chemical potential is smaller than the charge gap, the system remains an insulator. A transition to a metallic phase is expected to occur for ε_F of the order of Δ_c, i.e., for $t^2 \approx (Ut'^3)^{1/2} \exp(-2\pi t'/U)$. A qualitative sketch of the phase diagram is given in Fig. 11.

IV. SPIN-CHARGE SEPARATION

A. Spin and charge densities

Valuable insight into the nature of the insulator-metal transition can be obtained by studying the charge density distribution in the ground state and the spin-density distribution in the triplet excited state. The local density deviation

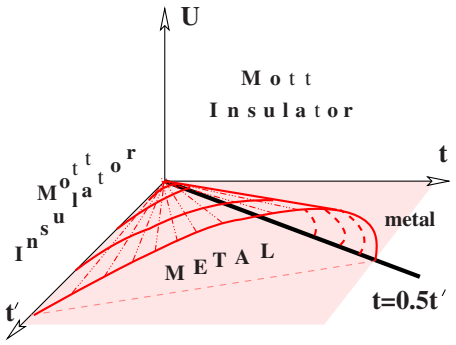

FIG. 11. (Color online) Qualitative phase diagram of the half-filled repulsive t-t' Hubbard chain. A gapless charge excitation spectrum (metallic phase) exists at $U=0$ for arbitrary t and t' and for $U>0$ in the sector of parameter space below the "roof" covering the area $U<U_c$ between the lines $t'=0.5t$ and $t=0$ in the $U=0$ plane.

$\langle n_\ell \rangle - \langle n \rangle$ on site ℓ and its Fourier transformation

$$\langle N_q \rangle \equiv \sum_\ell e^{-iq\ell} (\langle n_\ell \rangle - \langle n \rangle) \tag{20}$$

yields information about the spatial and momentum components present in the ground state of a system with open boundary conditions because the ends behave like impurities which produce Friedel oscillations.[31,32] Similar information about the lowest spin excited state in the triplet sector can be obtained by examining $\langle S^z_\ell \rangle$ and its Fourier transform $\langle S^z_q \rangle$, defined analogously to Eq. (20).

The Fourier transform of the charge distribution is shown in Fig. 12 for $U=3$, an intermediate interaction strength, as a function of t'. For $t'<0.6$, there are no significant fluctuations in the local charge density, as would be expected in one-chain picture ($\langle n_\ell \rangle = 1$ for all ℓ at $t'=0$). At $t' \approx 0.6$ and larger, we see the development of peaks near $q=0$ and $q=\pi$ which rapidly and symmetrically shift to higher and lower q values, respectively, with increasing t', going asymptotically toward $q=\pi/2$ for large values of t'. These peaks reflect scattering processes at $2k_F^-$ (low q) and $2k_F^+$ (high q). Above $t' \approx 0.9$, an additional peak at $q=\pi/2$ devel-

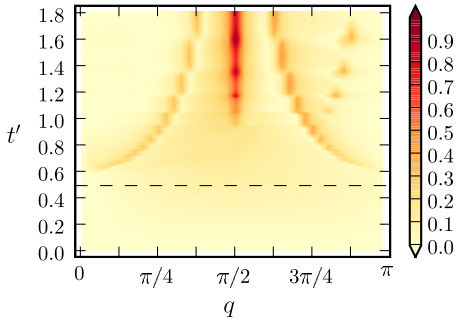

FIG. 12. (Color online) Density plot of the Fourier transform of the charge distribution $|\langle N_q \rangle|$ as a function of t' (vertical axis) for $U=3$ on an $L=80$ lattice.

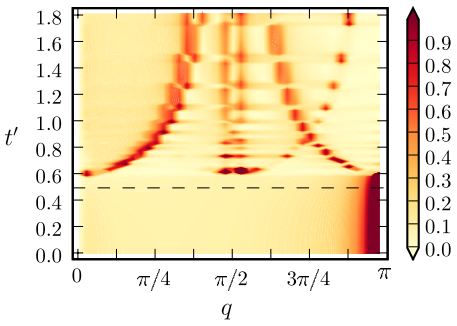

FIG. 13. (Color online) Density plot of the Fourier transform of the spin distribution $|\langle S^z_q\rangle|$ in the S^z=1 state with lowest energy for U=3 on an L=80 lattice.

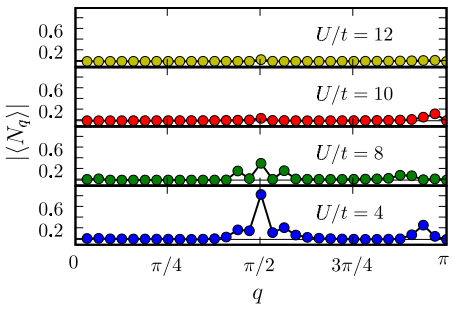

FIG. 14. (Color online) Fourier transform of the charge distribution $|\langle N_q\rangle|$ in the ground state of the t-t'-U chain with L=64, t' =3t, and U/t=4,8,10,20.

ops, quickly becoming dominant as t' is further increased. This peak is at the wave vector associated with scattering between the Fermi points, $k_F^+ - k_F^-$.

The behavior of the Fourier transform of the local spin density $|\langle S^z_q\rangle|$ of the ground state in the S^z=1 sector is depicted in Fig. 13. For $t' \approx 0.5t$ and smaller, there is a single well-defined peak at $q=q^*$ slightly less than π. This is due to the soliton-antisoliton pair that makes up the lowest triplet excitation in a single-chain picture, and is present in the Heisenberg chain. We expect q^* to shift closer and closer to π with system size because the size of the soliton-antisoliton pair is constrained by the number of sites. At $t' \approx 0.6$, this peak disappears rapidly with t' and is then replaced with a pattern of weaker peaks similar to those appearing in $|\langle N_q\rangle|$; compare with Fig. 12. The peaks starting near q=0 and q =π can again be attributed to $2k_F^-$ and $2k_F^+$ scattering processes. The peaks near $q=\pi/2$ are associated with scattering with wave vector $q=k_F^+ - k_F^-$.

Also evident in Fig. 13 are regular patterns as a function of t'. There are regular steplike structures in $|\langle S^z_q\rangle|$ as a function of t'. At the steps, there are interruptions in density, also marked by the appearance of peaks at additional scattering vectors. These effects are due to commensurability between the available low-lying scattering wave vectors, which change with t' and U, and the system size. In other words, when the appropriate wavelength of the excitation is commensurate with the system size, there is a shift and mirroring of the strongly weighted q points. This corresponds to a qualitatively more commensurate behavior of $\langle S^z_i\rangle$, as viewed in real space. These effects are also closely related to the irregular finite-size scaling of the spin gap, as seen in Fig. 9 for larger values of t'. Note that weaker, but analogous effects are also present in the charge density $|\langle N_q\rangle|$, Fig. 12.

B. Two-chain behavior

We examine the behavior of the t-t'-U chain for large next-nearest hopping ($t' \gg t$), a limit which corresponds to two chains coupled with a weak zigzag hopping. In particular, we numerically investigate the transition from a two-chain (four-Fermi-point) metallic regime at weak U to the strong-coupling regime, for which the effective model is two spin-S=1/2 Heisenberg chains coupled with a frustrating zigzag interaction at $U \gg t' \gg t$, i.e., $J' \gg J$.

In Fig. 14, we show the Fourier transform $\langle N_q\rangle$ of the charge distribution in the ground state of the t-t'-U chain at U=4,8,10,12 for t'=3t. In the metallic phase (U/t=4 and U/t=8), the strongest peak is at $q=\pi/2$, which corresponds to alternating charge density along each chain. In addition, there are side peaks which are due to weak alternations between the chains, as well as an incommensurate peak near $q=\pi$ due to asymmetric end effects on the two different chains, which shifts toward smaller q and becomes weaker as U is increased. As U/t is increased to 10, the amplitude of the charge fluctuations between the chains is strongly suppressed, as seen in the near disappearance of the peak at q =$\pi/2$. This indicates the transition to the insulating phase. The peak near $q=\pi$ now moves toward larger q, but becomes yet weaker with U. Deeper into the insulating phase, at U/t=12, the Fourier transform of the charge density is almost featureless, corresponding to a real-space charge density which is smooth and equal between the chains.

In Fig. 15, we show the Fourier transform of the spin-density distribution $\langle S^z_q\rangle$ in the $S^z_{\rm total}$=1 state for t'=3t and U/t=4,8,10,20. As can be seen, the weak incommensurate peaks on either side of $q=\pi/2$ present for U/t=4 and 8 become sharper and move toward $q=\pi/2$ as U is increased. These large-U excitations correspond to two-spinon excitations, as seen in the single Heisenberg chain,[33] in each chain. This behavior, also seen in the frustrated Heisenberg chain at

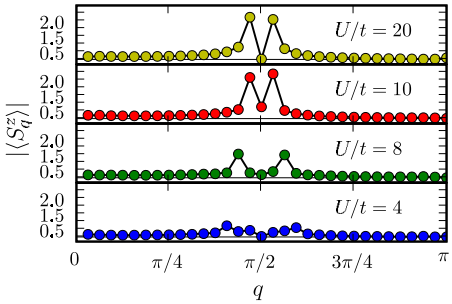

FIG. 15. (Color online) Fourier transform of the spin distribution $|\langle S^z_i\rangle|$ in the $S^z_{\rm total}$=1 state of the t-t'-U chain with L=64, t' =3t, and U/t=4,8,10,20.

large J'/J, indicates that the system behaves as two weakly coupled $S=1/2$ Heisenberg chains at large U.

V. CONCLUSIONS

We have carried out a combined analytical and numerical analysis of the insulator-metal transition in the half-filled one-dimensional t-t'-U model. Using the weak-coupling bosonization approach, we have shown that the gross features of the transition from an insulator to metal as a function of next-nearest-neighbor hopping t' can be described within the standard theory of commensurate-incommensurate transitions. We have derived an explicit expression for the critical line $t'_c(U)$ separating the metallic phase from the spin-gapped insulator.

Using DMRG calculations on chains of up to $L=128$ sites, we have performed a detailed numerical analysis of the excitation spectrum and the charge and spin-density distributions in various sectors of the phase diagram. In particular, we have studied the evolution of the charge and spin gap with increasing next-nearest-neighbor hopping amplitude t'. We have found evidence for a spin gap in the parameter range $0.5t<t'<t'_c$, in agreement with previous studies. We have shown that the change in the topology of Fermi surface at the insulator-metal transition is reflected in the appearance of incommensurate modulations of the charge density. Incommensurate spin-density distributions in the triplet sector are always present in the metallic phase, but can also appear independently in the spin-gapped insulator due to frustration.

For $t' \gg t$, we have argued that the insulator-metal transition can be best understood starting from the limit of two uncoupled chains. At small U, turning on the zigzag coupling between the chains destroys the commensurability present for a single chain, and leads to a metallic phase. At large U, the system is insulating and behaves as two weakly coupled Heisenberg chains. We have estimated that the insulator-metal transition in this regime occurs when the shift in the Fermi energy is comparable to the size of the charge gap in the isolated Hubbard chain.

ACKNOWLEDGMENTS

It is a pleasure to thank A. Aligia, C. Gros, A. Kampf, B. Normand, D. Poilblanc, and M. Sekania for interesting discussions. G.I.J. is grateful to the Max-Planck-Institut for Physics of Complex System, where part of this work has been performed, for support and warm hospitality. G.I.J. also acknowledges support from the STCU through Grant No. N3867. D.B. and G.I.J. also acknowledge support through SCOPES Grant No. 7GEPJ62379.

[1] N. F. Mott, *Metal-Insulator Transitions* 2nd ed. (Taylor and Francis, London, 1990).
[2] F. Gebhard, *The Mott Metal-Insulator Transition* (Springer, Berlin, 1997).
[3] M. Imada, A. Fujimori, and Y. Tokura, Rev. Mod. Phys. **70**, 1039 (1998).
[4] M. Dzierzawa, D. Baeriswyl, and L. M. Martelo, Helv. Phys. Acta **70**, 124 (1997).
[5] E. H. Lieb and F. Y. Wu, Phys. Rev. Lett. **20**, 1445 (1968).
[6] A. A. Ovchinnikov, Sov. Phys. JETP **30**, 1160 (1970).
[7] For a recent review, see F. H. L. Essler, H. Frahm, F. Göhmann, A. Klümper, and V. E. Korepin, *The One-Dimensional Hubbard Model* (Cambridge University Press, Cambridge, 2005).
[8] M. Fabrizio, Phys. Rev. B **54**, 10054 (1996).
[9] K. Kuroki, R. Arita, and H. Aoki, J. Phys. Soc. Jpn. **66**, 3371 (1997).
[10] S. Daul and R. M. Noack, Phys. Rev. B **58**, 2635 (1998).
[11] R. Arita, K. Kuroki, H. Aoki, and M. Fabrizio, Phys. Rev. B **57**, 10324 (1998).
[12] S. Daul and R. M. Noack, Phys. Rev. B **61**, 1646 (2000).
[13] M. E. Torio, A. A. Aligia, and H. A. Ceccatto, Phys. Rev. B **67**, 165102 (2003).
[14] C. Aebischer, D. Baeriswyl, and R. M. Noack, Phys. Rev. Lett. **86**, 468 (2001).
[15] K. Louis, J. V. Alvarez, and C. Gros, Phys. Rev. B **64**, 113106 (2001); **65**, 249903(E) (2002).
[16] K. Hamacher, C. Gros, and W. Wenzel, Phys. Rev. Lett. **88**, 217203 (2002).
[17] C. Gros, K. Hamacher, and W. Wenzel, Europhys. Lett. **69**, 616 (2005).
[18] M. Capello, F. Becca, M. Fabrizio, S. Sorella, and E. Tosatti, Phys. Rev. Lett. **94**, 026406 (2005).
[19] G. I. Japaridze and A. A. Nersesyan, JETP Lett. **27**, 356 (1978); JETP Lett. **27**, 334 (1978); J. Low Temp. Phys. **37**, 95 (1979); V. L. Pokrovsky and A. L. Talapov, Phys. Rev. Lett. **42**, 65 (1979); H. J. Schulz, Phys. Rev. B **22**, 5274 (1980).
[20] H. Q. Lin and J. E. Hirsch, Phys. Rev. B **35**, 3359 (1987).
[21] F. D. M. Haldane, Phys. Rev. B **25**, 4925 (1982); Phys. Rev. B **26**, 5257(E) (1982).
[22] K. Okamoto and K. Nomura, Phys. Lett. A **169**, 422 (1992); S. Eggert, Phys. Rev. B **54**, R9612 (1996).
[23] S. R. White and I. Affleck, Phys. Rev. B **54**, 9862 (1996).
[24] L. Balents and M. P. A. Fisher, Phys. Rev. B **53**, 12133 (1996).
[25] A. O. Gogolin, A. A. Nersesyan, and A. M. Tsvelik, *Bosonization and Strongly Correlated Systems* (Cambridge University Press, Cambridge, 1998).
[26] T. Giamarchi, *Quantum Physics in One Dimension* (Clarendon, Oxford 2004).
[27] G. I. Japaridze, A. A. Nersesyan, and P. B. Wiegmann, Nucl. Phys. B **230**, 511 (1984).
[28] For details, we refer to Bosonization and Strongly Correlated Systems (Ref. 25), Chap. 17.
[29] S. R. White, Phys. Rev. Lett. **69**, 2863 (1992); Phys. Rev. B **48**, 10345 (1993).
[30] C. Aebischer, Ph.D. thesis, University of Fribourg, 2002; available at http://ethesis.unifr.ch/theses
[31] M. Fabrizio and A. O. Gogolin, Phys. Rev. B **51**, 17827 (1995).
[32] G. Bedürftig, B. Brendel, H. Frahm, and R. M. Noack, Phys. Rev. B **58**, 10225 (1998).
[33] E. Sorensen, I. Affleck, D. Augier, and D. Poilblanc, Phys. Rev. B **58**, R14701 (1998).